Mech Time-Depend Mater (2017) 21:307–329
DOI 10.1007/s11043-016-9331-y

Three-dimensional elasticity solution of layered plates with viscoelastic interlayers

Peng Wu[1] · Ding Zhou[1,2] · Weiqing Liu[1] · Weidong Lu[1] · Li Wan[1]

Received: 26 May 2016 / Accepted: 20 September 2016 / Published online: 11 October 2016

Abstract An analytical solution for simply supported layered plates with viscoelastic interlayers under a transverse load is proposed. The deformation of each plate layer is described by the exact three-dimensional elasticity equations. The viscoelastic property of interlayer is simulated by the generalized Maxwell model. The constitutive relation of the interlayer is simplified by the quasi-elastic approximation, which significantly simplifies the analytical process. The solution of stress and displacement fields with undetermined coefficients is derived by solving a group of ordinary differential equations. The undetermined coefficients can be efficiently deduced by using the recursive matrix technique for the plate with any number of layers. The practical convergence is observed during numerical tests. The comparison analysis indicates that the present solution has a close agreement with the finite element solution. However, the solution based on the Mindlin–Reissner hypothesis is significantly different from the present solution for thick plates. Finally, the effect of interlayer thickness on stress and displacement distributions of a five-layer plate is discussed in detail.

Keywords Elasticity theory · Layered plate · Viscoelastic interlayer · Quasi-elastic model · Recursive matrix technique

✉ D. Zhou
dingzhou57@yahoo.com

P. Wu
wupeng2015@yahoo.com

W. Liu
wqliu@njtech.edu.cn

W. Lu
concrete@163.com

L. Wan
wanli@njtech.edu.cn

[1] College of Civil Engineering, Nanjing Tech University, Nanjing 211816, P.R. China

[2] Faculty of Architecture and Civil Engineering, Huaiyin Institute of Technology, Huaian 223300, P.R. China

1 Introduction

Layered structures are extensively used in different branches of mechanical and civil engineering. In addition to high strength, high stiffness and low density, another important advantage of layered structures is that their mechanical behavior can be tailored by changing material type of layers and layer number. The common applications are steel–concrete structures (Shafaei et al. 2016; Hu et al. 2016; Yan et al. 2016; Othman and Marzouk 2016), fiber reinforced polymers strengthened concrete structures (Xu et al. 2015; Teng et al. 2015; Neto et al. 2016; Hadigheh and Gravina 2016), laminated glass structures (Foraboschi 2012; Zhu and Khanna 2016; Del Linz et al. 2016), and so on. The character of connection between adjacent layers has a great effect on the mechanical property of layered structures. If adjacent layers are connected by rigid connectors, perfect connection can be obtained. However, the rigid connectors can hardly be realized in practice. The common connectors, like nails, dowels, studs, structural adhesives, and so on, can only provide finite stiffness. Therefore, interfacial slip often occurs in layered structures. Because the structural adhesives possess viscoelastic property, the mechanical behavior of interfacial bonding between adjacent layers is essentially time-dependent. Some investigators studied layered beams with viscoelastic interlayer (Zhang and Wang 2011; Galuppi and Royer-Carfagni 2012, 2014; Li et al. 2014; Wu et al. 2016a, 2016b). However, researches on layered plates with viscoelastic interlayer are rare.

The classical plate theory (CPT) based on the well-known Kirchhoff–Love hypothesis (Kirchhoff 1850) is recognized as the most popular theory for plates. By use of the CPT, various static and dynamic problems of plates were studied. Foraboschi (2013a, 2014) presented analytical solutions for simply-supported three-layered plate, composed of two relatively stiff outer layers and a more compliant interlayer, subjected to a transverse load. The outer layers behave following the Kirchhoff–Love hypothesis. A homogenized Kirchhoff–Love model was developed by Dallot and Sab (2008) for limit analysis of multi-layered plates. By use of a modified couple stress theory, Thai and Choi (2013) developed size-dependent models for bending, buckling, and vibration problems of functionally graded plates. A frequency-domain spectral element model was developed by Park and Lee (2015) to analyze transverse vibration of a symmetric laminated plate. An analytical model for two-layer plate with discontinuous interfacial connection was investigated by Foraboschi (2013b).

However, the CPT neglects the transverse shear deformation, which is increasingly important when the plate becomes thicker. Therefore, it may lead to inaccurate results for thick plates. In order to consider the transverse shear deformation, the first-order shear deformation theory (FSDT) was developed to analyze moderately thick plates. This theory assumes the transverse shear strains to be constant through the thickness during deformation and a shear correction factor is used to adjust the transverse shear stiffness (Reissner 1945; Mindlin 1951). Bending behavior and stress analysis of angle-ply laminated and sandwich plates under arbitrary distributed loads were studied by Alipour (2016) using the FSDT. Romanoff and Varsta (2007) presented bending response of web-core sandwich plates, in which the discrete core was transformed into an equivalent homogenous continuous one. Using adjusted differential evolution algorithm and smoothed triangular plate element, Le-Anh et al. (2015) proposed a coupled numerical method for static optimization of folded laminated plates. Golmakani and Mehrabian (2014) tackled bending problem of annular general angle-ply laminated plates subjected to a transverse load with various boundary conditions. Mantari and Ore (2015) developed a simplified FSDT, with a new displacement field containing only four unknowns and gave the Navier-type close-form solution for free

vibration of sandwich plates. Based on the Hamilton's principle, damping effect of composite plate with viscoelastic mid-layer was analyzed by Yang et al. (2016). The viscoelastic behavior of the mid-layer was described by the hysteric damping model. Since the shear correction factor in FSDT depends on boundary conditions, material and geometric parameters, it is difficult to be accurately deduced. In order to improve the accuracy, higher-order shear deformation theories (HSDTs), which assume shear strain to be nonlinearly distributed through the thickness, have been developed. Some typical HSDTs were proposed by Reddy (1984), Khdeir (1988), Matsunaga (2000), Kant and Swaminathan (2002), Ferreira et al. (2003), Swaminathan and Patil (2007), Kim et al. (2009), etc.

Three-dimensional elasticity theory (3DET) is always recognized as a benchmark for comparisons, since it renounces any transverse shear deformation hypothesis. Pagano (1969, 1970) presented analytical solutions for laminate plates composed of arbitrary numbers of layers. Bending, buckling and vibration of simply supported thick laminate plates were investigated by Srinivas and Rao (1970). Williams and Addessio (1997) extended Pagano's work (1969) to laminate plates with delamination. Using p-Ritz method, Wang et al. (2000) tackled free vibration for skew sandwich plates composed of two laminated facings sandwiching an orthotropic core. Though the 3DET can provide accurate results for plates with any thickness, it is often computationally expensive, especially for laminated plates with a large number of layers. Asymptotic approach based on 3DET was used to investigate mechanical behavior of thin-walled elastic bodies by Reissner (1980), Gregory and Wan (1993), and Kaplunov et al. (1998).

In this work, a new analytical method based on the 3DET is presented to study simply supported layered plates with viscoelastic interlayer under an arbitrary distributed load. The plate layers behave according to the 3DET. The viscoelastic interlayer between adjacent layers is simulated by the generalized Maxwell model, and its constitutive relation is simplified by the quasi-elastic approximation. The present solution can be efficiently obtained by use of the recursive matrix technique, even if the number of the plate layers is large. The present solution can provide accurate results of stress and displacement distribution, which cannot be provided by the simplified solution such as the one based on the Mindlin–Reissner hypothesis.

2 Analytical model

As shown in Fig. 1, a simply supported layered plate with length a, width b, and total thickness h is considered, which is made of p elastic layers with thickness h_i adhesively bonded by $p-1$ viscoelastic interlayers with the same thickness Δh, subjected to a distributed load $q(x, y)$ on the top surface of the plate. Two Cartesian coordinate systems are established to describe the plate and layers respectively, global Cartesian coordinates o-xyz with origin o at the bottom of the plate and local Cartesian coordinates o_i-xyz_i with origin o_i at the bottom of ith layer.

2.1 Assumptions

The analytical process of the layered plate with viscoelastic interlayer keeps the following assumptions:

(1) The deformation of the layered plate is within the extent of linear elasticity.

(2) The interlayer thickness is very small compared to the layer thickness, i.e., $\Delta h \ll h_i$.

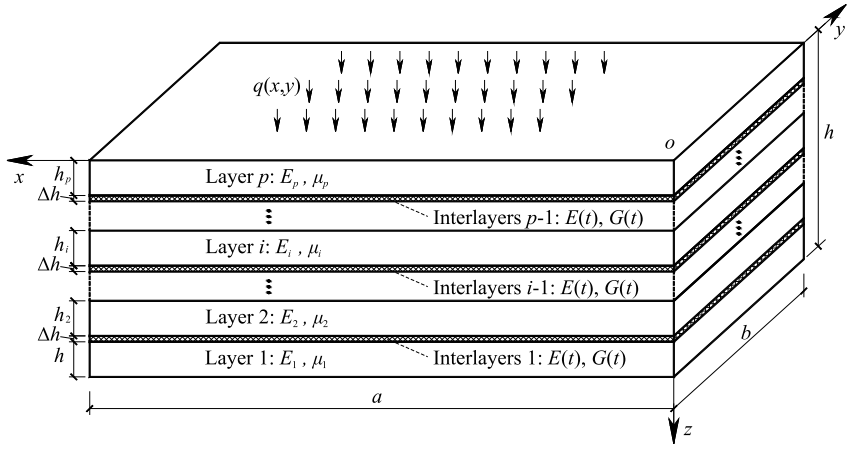

(a) Global Cartesian coordinate

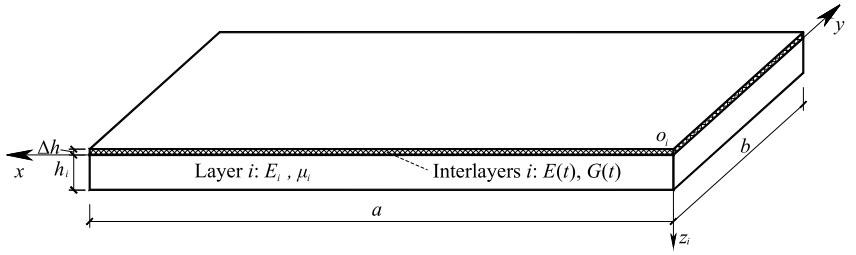

(b) Local Cartesian coordinate

Fig. 1 Simply supported layered plate with viscoelastic interlayer

(3) The adhesive interlayer is thin and soft. Its capacity to bear x-directional and y-directional normal stresses is weak. Therefore, the x-directional and y-directional normal stresses in the interlayer are negligible.

(4) The displacements in the interlayer are considered to be linearly distributed through the thickness. Therefore, the strains through the interlayer thickness are constants.

2.2 Equations for a plate layer

The ith layer of the plate is considered within the local Cartesian coordinates o_i-xyz_i. According to the 3DET, the constitutive relations for ith layer are

$$\begin{aligned}
\sigma_x^{(i)} &= (\lambda_i + 2G_i)\varepsilon_x^{(i)} + \lambda_i\varepsilon_y^{(i)} + \lambda_i\varepsilon_{z_i}^{(i)},\\
\sigma_y^{(i)} &= \lambda_i\varepsilon_x^{(i)} + (\lambda_i + 2G_i)\varepsilon_y^{(i)} + \lambda_i\varepsilon_{z_i}^{(i)},\\
\sigma_{z_i}^{(i)} &= \lambda_i\varepsilon_x^{(i)} + \lambda_i\varepsilon_y^{(i)} + (\lambda_i + 2G_i)\varepsilon_{z_i}^{(i)},\\
\tau_{yz_i}^{(i)} &= G_i\gamma_{yz_i}^{(i)}, \qquad \tau_{xz_i}^{(i)} = G_i\gamma_{yz_i}^{(i)}, \qquad \tau_{xy}^{(i)} = G_i\gamma_{xy}^{(i)}, \quad i = 1, 2, \ldots, p,
\end{aligned} \tag{1}$$

in which $\sigma_x^{(i)}$, $\sigma_y^{(i)}$, $\sigma_{z_i}^{(i)}$, $\tau_{yz_i}^{(i)}$, $\tau_{xz_i}^{(i)}$, and $\tau_{xy}^{(i)}$ are stress components, $\varepsilon_x^{(i)}$, $\varepsilon_y^{(i)}$, $\varepsilon_{z_i}^{(i)}$, $\gamma_{yz_i}^{(i)}$, $\gamma_{yz_i}^{(i)}$, and $\gamma_{xy}^{(i)}$ are strain components. The symbols λ_i and G_i are Lame constants, which are given

by

$$\lambda_i = \frac{\mu_i E_i}{(1+\mu_i)(1-2\mu_i)}, \qquad G_i = \frac{E_i}{2(1+\mu_i)}, \quad i = 1, 2, \ldots, p, \tag{2}$$

where E_i and μ_i denote elastic modulus and Poisson's ratio of the ith layer, respectively. The geometrical relations of the ith layer are

$$\begin{aligned}
&\varepsilon_x^{(i)} = \frac{\partial u^{(i)}}{\partial x}, \qquad \varepsilon_y^{(i)} = \frac{\partial v^{(i)}}{\partial y}, \qquad \varepsilon_{z_i}^{(i)} = \frac{\partial w^{(i)}}{\partial z_i},\\
&\gamma_{yz_i}^{(i)} = \frac{\partial v^{(i)}}{\partial z_i} + \frac{\partial w^{(i)}}{\partial y}, \qquad \gamma_{xz_i}^{(i)} = \frac{\partial u^{(i)}}{\partial z_i} + \frac{\partial w^{(i)}}{\partial x},\\
&\gamma_{xy}^{(i)} = \frac{\partial u^{(i)}}{\partial y} + \frac{\partial v^{(i)}}{\partial x}, \quad i = 1, 2, \ldots, p,
\end{aligned} \tag{3}$$

where $u^{(i)}$, $v^{(i)}$, and $w^{(i)}$ respectively represent the displacement components in the x, y, and z directions. The equilibrium equations of the ith layer, in the absence of body forces, are described by

$$\begin{aligned}
&\frac{\partial \sigma_x^{(i)}}{\partial x} + \frac{\partial \tau_{xy}^{(i)}}{\partial y} + \frac{\partial \tau_{xz_i}^{(i)}}{\partial z_i} = 0, \qquad \frac{\partial \sigma_y^{(i)}}{\partial y} + \frac{\partial \tau_{xy}^{(i)}}{\partial x} + \frac{\partial \tau_{yz_i}^{(i)}}{\partial z_i} = 0,\\
&\frac{\partial \sigma_{z_i}^{(i)}}{\partial z_i} + \frac{\partial \tau_{xz_i}^{(i)}}{\partial x} + \frac{\partial \tau_{yz_i}^{(i)}}{\partial y} = 0, \quad i = 1, 2, \ldots, p.
\end{aligned} \tag{4}$$

Because of the viscoelasticity of the interlayer, the stress, strain, and displacement components of the plate are time-dependent in nature. Substituting Eq. (3) into Eq. (1) yields

$$\begin{aligned}
&\sigma_x^{(i)} = (\lambda_i + 2G_i)\frac{\partial u^{(i)}}{\partial x} + \lambda_i \frac{\partial v^{(i)}}{\partial y} + \lambda_i \frac{\partial w^{(i)}}{\partial z_i}, \qquad \tau_{yz_i}^{(i)} = G_i\left(\frac{\partial v^{(i)}}{\partial z_i} + \frac{\partial w^{(i)}}{\partial y}\right),\\
&\sigma_y^{(i)} = \lambda_i \frac{\partial u^{(i)}}{\partial x} + (\lambda_i + 2G_i)\frac{\partial v^{(i)}}{\partial y} + \lambda_i \frac{\partial w^{(i)}}{\partial z_i}, \qquad \tau_{xz_i}^{(i)} = G_i\left(\frac{\partial u^{(i)}}{\partial z_i} + \frac{\partial w^{(i)}}{\partial x}\right),\\
&\sigma_{z_i}^{(i)} = \lambda_i \frac{\partial u^{(i)}}{\partial x} + \lambda_i \frac{\partial v^{(i)}}{\partial y} + (\lambda_i + 2G_i)\frac{\partial w^{(i)}}{\partial z_i}, \qquad \tau_{xy}^{(i)} = G_i\left(\frac{\partial u^{(i)}}{\partial y} + \frac{\partial v^{(i)}}{\partial x}\right),\\
&i = 1, 2, \ldots, p.
\end{aligned} \tag{5}$$

Substituting Eq. (5) into Eq. (4) leads to a group of differential equations, as follows:

$$\begin{aligned}
&G_i\left(\frac{\partial^2 u^{(i)}}{\partial x^2} + \frac{\partial^2 u^{(i)}}{\partial y^2} + \frac{\partial^2 u^{(i)}}{\partial z_i^2}\right) + (\lambda_i + G_i)\left(\frac{\partial^2 u^{(i)}}{\partial x^2} + \frac{\partial^2 v^{(i)}}{\partial x \partial y} + \frac{\partial^2 w^{(i)}}{\partial x \partial z_i}\right) = 0,\\
&G_i\left(\frac{\partial^2 v^{(i)}}{\partial x^2} + \frac{\partial^2 v^{(i)}}{\partial y^2} + \frac{\partial^2 v^{(i)}}{\partial z_i^2}\right) + (\lambda_i + G_i)\left(\frac{\partial^2 u^{(i)}}{\partial x \partial y} + \frac{\partial^2 v^{(i)}}{\partial y^2} + \frac{\partial^2 w^{(i)}}{\partial y \partial z_i}\right) = 0,\\
&G_i\left(\frac{\partial^2 w^{(i)}}{\partial x^2} + \frac{\partial^2 w^{(i)}}{\partial y^2} + \frac{\partial^2 w^{(i)}}{\partial z_i^2}\right) + (\lambda_i + G_i)\left(\frac{\partial^2 u^{(i)}}{\partial x \partial z_i} + \frac{\partial^2 v^{(i)}}{\partial y \partial z_i} + \frac{\partial^2 w^{(i)}}{\partial z_i^2}\right) = 0,\\
&i = 1, 2, \ldots, p.
\end{aligned} \tag{6}$$

The boundary conditions of four simply supported edges are

$$\sigma_x^{(i)} = v^{(i)} = w^{(i)} = 0, \quad \text{at } x = 0, a,$$
$$\sigma_y^{(i)} = u^{(i)} = w^{(i)} = 0, \quad \text{at } y = 0, b, \ i = 1, 2, \ldots, p. \tag{7}$$

For simply supported plates, the displacement components can be expressed as double Fourier series as follows:

$$u^{(i)}(x, y, z_i, t) = \sum_{m=1}^{\infty}\sum_{n=1}^{\infty} U_{mn}^{(i)}(z_i, t)\cos(\alpha_m x)\sin(\beta_n y),$$
$$v^{(i)}(x, y, z_i, t) = \sum_{m=1}^{\infty}\sum_{n=1}^{\infty} V_{mn}^{(i)}(z_i, t)\sin(\alpha_m x)\cos(\beta_n y),$$
$$w^{(i)}(x, y, z_i, t) = \sum_{m=1}^{\infty}\sum_{n=1}^{\infty} W_{mn}^{(i)}(z_i, t)\sin(\alpha_m x)\sin(\beta_n y), \quad i = 1, 2, \ldots, p, \tag{8}$$

where $\alpha_m = m\pi/a$, $\beta_n = n\pi/b$. Substituting Eq. (8) into Eq. (6) gives

$$\begin{aligned}
&G_i\left[\frac{\partial^2 U_{mn}^{(i)}(z_i, t)}{\partial z_i^2} - (\beta_n)^2 U_{mn}^{(i)}(z_i, t)\right] - (\alpha_m)^2(\lambda_i + 2G_i)U_{mn}^{(i)}(z_i, t) \\
&\quad - \alpha_m\beta_n(\lambda_i + G_i)V_{mn}^{(i)}(z_i, t) + \alpha_m(\lambda_i + G_i)\frac{\partial W_{mn}^{(i)}(z_i, t)}{\partial z_i} = 0, \\
&G_i\left[\frac{\partial^2 V_{mn}^{(i)}(z_i, t)}{\partial z_i^2} - (\alpha_m)^2 V_{mn}^{(i)}(z_i, t)\right] - (\beta_n)^2(\lambda_i + 2G_i)V_{mn}^{(i)}(z_i, t) \\
&\quad - \alpha_m\beta_n(\lambda_i + G_i)U_{mn}^{(i)}(z_i, t) + \beta_n(\lambda_i + G_i)\frac{\partial W_{mn}^{(i)}(z_i, t)}{\partial z_i} = 0, \\
&(\lambda_i + 2G_i)\frac{\partial^2 W_{mn}^{(i)}(z_i, t)}{\partial z_i^2} - G_i\left[(\alpha_m)^2 + (\beta_n)^2\right]W_{mn}^{(i)}(z_i, t) \\
&\quad - (\lambda_i + G_i)\alpha_m\frac{\partial U_{mn}^{(i)}(z_i, t)}{\partial z_i} - (\lambda_i + G_i)\beta_n\frac{\partial V_{mn}^{(i)}(z_i, t)}{\partial z_i} = 0, \\
&i = 1, 2, \ldots, p.
\end{aligned} \tag{9}$$

Solving the above ordinary differential equations, we have the solutions:

$$\begin{aligned}
u^{(i)}(x, y, z_i, t) = \sum_{m=1}^{\infty}\sum_{n=1}^{\infty} \beta_n\cos(\alpha_m x)\sin(\beta_n y)\Bigg[&\frac{\alpha_m}{\phi_{mn}} z_i \sinh(\phi_{mn} z_i)C_{mn}^{(i)}(t) \\
&+ \frac{\alpha_m}{\phi_{mn}} z_i \cosh(\phi_{mn} z_i)D_{mn}^{(i)}(t) + \cosh(\phi_{mn} z_i)E_{mn}^{(i)}(t) \\
&+ \sinh(\phi_{mn} z_i)F_{mn}^{(i)}(t)\Bigg],
\end{aligned}$$

$$
\begin{aligned}
v^{(i)}(x,y,z_i,t) = \sum_{m=1}^{\infty}\sum_{n=1}^{\infty} \sin(\alpha_m x)\cos(\beta_n y)\Big[& \phi_{mn}\sinh(\phi_{mn}z_i)A_{mn}^{(i)}(t) \\
& + \phi_{mn}\cosh(\phi_{mn}z_i)B_{mn}^{(i)}(t) \\
& + \left(\frac{\lambda_i+3G_i}{\lambda_i+G_i}\cosh(\phi_{mn}z_i) + \frac{(\beta_n)^2}{\phi_{mn}}z_i\sinh(\phi_{mn}z_i)\right)C_{mn}^{(i)}(t) \\
& + \left(\frac{\lambda_i+3G_i}{\lambda_i+G_i}\sinh(\phi_{mn}z_i) + \frac{(\beta_n)^2}{\phi_{mn}}z_i\cosh(\phi_{mn}z_i)\right)D_{mn}^{(i)}(t) \\
& - \alpha_m\cosh(\phi_{mn}z_i)E_{mn}^{(i)}(t) - \alpha_m\sinh(\phi_{mn}z_i)F_{mn}^{(i)}(t)\Big], \\
w^{(i)}(x,y,z_i,t) = \sum_{m=1}^{\infty}\sum_{n=1}^{\infty} \beta_n\sin(\alpha_m x)\sin(\beta_n y)\big[& \cosh(\phi_{mn}z_i)A_{mn}^{(i)}(t) \\
& + \sinh(\phi_{mn}z_i)B_{mn}^{(i)}(t) + z_i\cosh(\phi_{mn}z_i)C_{mn}^{(i)}(t) \\
& + z_i\sinh(\phi_{mn}z_i)D_{mn}^{(i)}(t)\big], \quad i=1,2,\ldots,p,
\end{aligned} \tag{10}
$$

where $\phi_{mn} = \sqrt{(\alpha_m)^2+(\beta_n)^2}$; $A_{mn}^{(i)}(t)$, $B_{mn}^{(i)}(t)$, $C_{mn}^{(i)}(t)$, $D_{mn}^{(i)}(t)$, $E_{mn}^{(i)}(t)$, and $F_{mn}^{(i)}(t)$ are the undetermined coefficients with respect to the time variable t. Substituting Eq. (10) into Eq. (5) yields the stress components

$$
\begin{aligned}
\sigma_x^{(i)}(x,y,z_i,t) = -\sum_{m=1}^{\infty}\sum_{n=1}^{\infty} & 2\beta_n G_i\sin(\alpha_m x)\sin(\beta_n y) \\
& \times\Bigg[\left(\frac{\lambda_i}{\lambda_i+G_i}\cosh(\phi_{mn}z_i) + \frac{(\alpha_m)^2}{\phi_{mn}}z_i\sinh(\phi_{mn}z_i)\right)C_{mn}^{(i)}(t) \\
& + \left(\frac{\lambda_i}{\lambda_i+G_i}\sinh(\phi_{mn}z_i) + \frac{(\alpha_m)^2}{\phi_{mn}}z_i\cosh(\phi_{mn}z_i)\right)D_{mn}^{(i)}(t) \\
& + \alpha_m\cosh(\phi_{mn}z_i)E_{mn}^{(i)}(t) + \alpha_m\sinh(\phi_{mn}z_i)F_{mn}^{(i)}(t)\Bigg], \\
\sigma_y^{(i)}(x,y,z_i,t) = -\sum_{m=1}^{\infty}\sum_{n=1}^{\infty} & 2\beta_n G_i\sin(\alpha_m x)\sin(\beta_n y) \\
& \times\Bigg[\phi_{mn}\sinh(\phi_{mn}z_i)A_{mn}^{(i)}(t) + \phi_{mn}\cosh(\phi_{mn}z_i)B_{mn}^{(i)}(t) \\
& + \left(\frac{2\lambda_i+3G_i}{\lambda_i+G_i}\cosh(\phi_{mn}z_i) + \frac{(\beta_n)^2}{\phi_{mn}}z_i\sinh(\phi_{mn}z_i)\right)C_{mn}^{(i)}(t) \\
& + \left(\frac{2\lambda_i+3G_i}{\lambda_i+G_i}\sinh(\phi_{mn}z_i) + \frac{(\beta_n)^2}{\phi_{mn}}z_i\cosh(\phi_{mn}z_i)\right)D_{mn}^{(i)}(t) \\
& - \alpha_m\cosh(\phi_{mn}z_i)E_{mn}^{(i)}(t) - \alpha_m\sinh(\phi_{mn}z_i)F_{mn}^{(i)}(t)\Bigg],
\end{aligned}
$$

$$\sigma_{z_i}^{(i)}(x,y,z_i,t)=\sum_{m=1}^{\infty}\sum_{n=1}^{\infty}2\beta_n G_i\sin(\alpha_m x)\sin(\beta_n y)$$
$$\times\Bigg[\phi_{mn}\sinh(\phi_{mn}z_i)A_{mn}^{(i)}(t)+\phi_{mn}\cosh(\phi_{mn}z_i)B_{mn}^{(i)}(t)$$
$$+\left(\frac{G_i}{\lambda_i+G_i}\cosh(\phi_{mn}z_i)+\phi_{mn}z_i\sinh(\phi_{mn}z_i)\right)C_{mn}^{(i)}(t)$$
$$+\left(\frac{G_i}{\lambda_i+G_i}\sinh(\phi_{mn}z_i)+\phi_{mn}z_i\cosh(\phi_{mn}z_i)\right)D_{mn}^{(i)}(t)\Bigg],$$

$$\tau_{xz_i}^{(i)}(x,y,z_i,t)=\sum_{m=1}^{\infty}\sum_{n=1}^{\infty}\beta_n G_i\cos(\alpha_m x)\sin(\beta_n y)$$
$$\times\Bigg[\alpha_m\cosh(\phi_{mn}z_i)A_{mn}^{(i)}(t)+\alpha_m\sinh(\phi_{mn}z_i)B_{mn}^{(i)}(t)$$
$$+\left(\frac{\alpha_m}{\phi_{mn}}\sinh(\phi_{mn}z_i)+2\alpha_m z_i\cosh(\phi_{mn}z_i)\right)C_{mn}^{(i)}(t)$$
$$+\left(\frac{\alpha_m}{\phi_{mn}}\cosh(\phi_{mn}z_i)+2\alpha_m z_i\sinh(\phi_{mn}z_i)\right)D_{mn}^{(i)}(t)$$
$$+\phi_{mn}\sinh(\phi_{mn}z_i)E_{mn}^{(i)}(t)+\phi_{mn}\cosh(\phi_{mn}z_i)F_{mn}^{(i)}(t)\Bigg],$$

$$\tau_{yz_i}^{(i)}(x,y,z_i,t)=\sum_{m=1}^{\infty}\sum_{n=1}^{\infty}G_i\sin(\alpha_m x)\cos(\beta_n y)$$
$$\times\Bigg\{\left[(\beta_n)^2+(\phi_{mn})^2\right]\cosh(\phi_{mn}z_i)A_{mn}^{(i)}(t)$$
$$+\left[(\beta_n)^2+(\phi_{mn})^2\right]\sinh(\phi_{mn}z_i)B_{mn}^{(i)}(t)$$
$$+\Bigg[\left(\frac{\lambda_i+3G_i}{\lambda_i+G_i}\phi_{mn}+\frac{(\beta_n)^2}{\phi_{mn}}\right)\sinh(\phi_{mn}z_i)$$
$$+2(\beta_n)^2 z_i\cosh(\phi_{mn}z_i)\Bigg]C_{mn}^{(i)}(t)$$
$$+\Bigg[\left(\frac{\lambda_i+3G_i}{\lambda_i+G_i}\phi_{mn}+\frac{(\beta_n)^2}{\phi_{mn}}\right)\cosh(\phi_{mn}z_i)$$
$$+2(\beta_n)^2 z_i\sinh(\phi_{mn}z_i)\Bigg]D_{mn}^{(i)}(t)$$
$$-\alpha_m\phi_{mn}\sinh(\phi_{mn}z_i)E_{mn}^{(i)}(t)-\alpha_m\phi_{mn}\cosh(\phi_{mn}z_i)F_{mn}^{(i)}(t)\Bigg\},$$

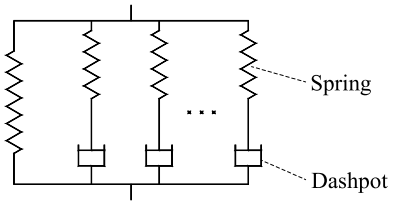

Fig. 2 Generalized Maxwell model

$$\tau_{xy}^{(i)}(x,y,z_i,t)=\sum_{m=1}^{\infty}\sum_{n=1}^{\infty}G_i\cos(\alpha_m x)\cos(\beta_n y)$$
$$\times\Bigg[\alpha_m\phi_{mn}\sinh(\phi_{mn}z_i)A_{mn}^{(i)}(t)+\alpha_m\phi_{mn}\cosh(\phi_{mn}z_i)B_{mn}^{(i)}(t)$$
$$+\left(\frac{\lambda_i+3G_i}{\lambda_i+G_i}\alpha_m\cosh(\phi_{mn}z_i)+\frac{2\alpha_m(\beta_n)^2}{\phi_{mn}}z_i\sinh(\phi_{mn}z_i)\right)C_{mn}^{(i)}(t)$$
$$+\left(\frac{\lambda_i+3G_i}{\lambda_i+G_i}\alpha_m\sinh(\phi_{mn}z_i)+\frac{2\alpha_m(\beta_n)^2}{\phi_{mn}}z_i\cosh(\phi_{mn}z_i)\right)D_{mn}^{(i)}(t)$$
$$+\left[(\beta_n)^2-(\alpha_m)^2\right]\cosh(\phi_{mn}z_i)E_{mn}^{(i)}(t)$$
$$+\left[(\beta_n)^2-(\alpha_m)^2\right]\sinh(\phi_{mn}z_i)F_{mn}^{(i)}(t)\Bigg],\quad i=1,2,\ldots,p. \tag{11}$$

One can find that no matter what values the undetermined coefficients in Eqs. (10) and (11) are prescribed, the simply supported boundary conditions in Eq. (7) have been rigorously satisfied.

2.3 Equations for an interlayer

The rheological models, consisting of springs and dashpots, are effective methods to simulate viscoelastic property (Neville et al. 1983). The classical Maxwell and Kelvin models provide the simple mathematical descriptions of viscoelastic property. The most commonly used model is the generalized Maxwell model, as shown in Fig. 2. By using the generalized Maxwell model, the time-dependent elastic modulus $E(t)$ and shear modulus $G(t)$ in the interlayer can be described by

$$E(t)=E_\infty+\sum_{j=1}^{k}E_j e^{-t/\theta_{E,j}},\qquad G(t)=G_\infty+\sum_{j=1}^{l}G_j e^{-t/\theta_{G,j}}, \tag{12}$$

where E_j and G_j are the relaxation elastic and shear modulus, respectively; E_∞ and G_∞ are the long-term elastic and shear modulus, respectively; $\theta_{E,j}$ and $\theta_{G,j}$ are the relaxation times. These viscoelastic parameters can be obtained through the creep or relaxation tests (Guedes et al. 1998; Arzoumanidis and Liechti 2003; Kim et al. 2008). Consider the ith interlayer within the local Cartesian coordinates o_i-xyz_i. According to Assumption 4 given in Sect. 2.1, the shear and normal strains in the interlayer are independent of the coordinate z_i. The constitutive relations of the interlayer can be described by the Boltzmann superposition

principle (Boltzmann 1874), as follows:

$$\begin{aligned}
\bar{\sigma}_{z_i}^{(i)}(x,y,t) &= E(t)\bar{\varepsilon}_{z_i}^{(i)}(x,y,0) + \int_0^t E(t-\xi)\frac{\partial \bar{\varepsilon}_{z_i}^{(i)}(x,y,\xi)}{\partial \xi}d\xi,\\
\bar{\tau}_{yz_i}^{(i)}(x,y,t) &= G(t)\bar{\gamma}_{yz_i}^{(i)}(x,y,0) + \int_0^t G(t-\xi)\frac{\partial \bar{\gamma}_{yz_i}^{(i)}(x,y,\xi)}{\partial \xi}d\xi,\\
\bar{\tau}_{xz_i}^{(i)}(x,y,t) &= G(t)\bar{\gamma}_{xz_i}^{(i)}(x,y,0) + \int_0^t G(t-\xi)\frac{\partial \bar{\gamma}_{xz_i}^{(i)}(x,y,\xi)}{\partial \xi}d\xi,\\
& i = 1,2,\ldots,p-1,
\end{aligned} \tag{13}$$

in which $\bar{\sigma}_{z_i}^{(i)}$, $\bar{\tau}_{yz_i}^{(i)}$, and $\bar{\tau}_{xz_i}^{(i)}$ denote the stress components in the interlayer; $\bar{\varepsilon}_{z_i}^{(i)}$, $\bar{\gamma}_{yz_i}^{(i)}$, and $\bar{\gamma}_{xz_i}^{(i)}$ denote the strain components in the interlayer. However, such full viscoelastic analysis is computationally expensive. The quasi-elastic approximation (Galuppi and Royer-Carfagni 2012, 2013), which assumes the viscoelastic material as a linear elastic one with time-dependent properties, is commonly used in practice. By use of the quasi-elastic approximation, Eq. (13) is simplified as

$$\begin{aligned}
&\bar{\sigma}_{z_i}^{(i)}(x,y,t) = E(t)\bar{\varepsilon}_{z_i}^{(i)}(x,y,t), \qquad \bar{\tau}_{xz_i}^{(i)}(x,y,t) = G(t)\bar{\gamma}_{xz_i}^{(i)}(x,y,t),\\
&\bar{\tau}_{yz_i}^{(i)}(x,y,t) = G(t)\bar{\gamma}_{yz_i}^{(i)}(x,y,t), \quad i = 1,2,\ldots,p-1.
\end{aligned} \tag{14}$$

One can find from Eq. (14) that the stress of viscoelastic material is only dependent on the current strain. The effect of strain history is neglected in the quasi-elastic approximation. For a given time, the analysis with parametric dependence on time is similar to the static one. Compared with the viscoelastic solution, the solution based on the quasi-elastic approximation is always on the side of safety for time-independent load (Galuppi and Royer-Carfagni 2012), while the quasi-elastic approximation may be unserviceable for time-dependent load with loading–unloading path (Galuppi and Royer-Carfagni 2013).

2.4 Loading conditions and consistent conditions

The undetermined coefficients in the stress and displacement components can be uniquely determined by the loading conditions as well as the consistent conditions between the layers and interlayers. The loading conditions on the surfaces of the plate are given by

$$\begin{aligned}
&\sigma_{z_1}^{(1)}(x,y,h_1,t) = 0, \qquad \tau_{xz_1}^{(1)}(x,y,h_1,t) = 0, \qquad \tau_{yz_1}^{(1)}(x,y,h_1,t) = 0,\\
&\sigma_{z_p}^{(p)}(x,y,0,t) = -q(x,y), \qquad \tau_{xz_p}^{(p)}(x,y,0,t) = 0, \qquad \tau_{y_p}^{(p)}(x,y,0,t) = 0.
\end{aligned} \tag{15}$$

Since the stress and displacement components are all expressed by double Fourier series, the load $q(x,y)$ is also expanded into series form as follows:

$$q(x,y) = \frac{4}{ab}\sum_{m=1}^{\infty}\sum_{n=1}^{\infty}\left[\int_0^a\int_0^b q(x,y)\sin(\alpha_m x)\sin(\beta_n y)\mathrm{d}x\mathrm{d}y\right]\sin(\alpha_m x)\sin(\beta_n y). \tag{16}$$

The consistent conditions for stresses are given as follows:

$$\sigma_{z_i}^{(i)}(x,y,0,t) = \bar{\sigma}_{z_i}^{(i)}(x,y,t) = \sigma_{z_{i+1}}^{(i+1)}(x,y,h_{i+1},t),$$

$$\tau_{xz_i}^{(i)}(x,y,0,t)=\bar{\tau}_{xz_i}^{(i)}(x,y,t)=\tau_{xz_{i+1}}^{(i+1)}(x,y,h_{i+1},t),$$
$$\tau_{yz_i}^{(i)}(x,y,0,t)=\bar{\tau}_{yz_i}^{(i)}(x,y,t)=\tau_{yz_{i+1}}^{(i+1)}(x,y,h_{i+1},t),\quad i=1,2,\ldots,p-1. \tag{17}$$

According to Assumption 4 in Sect. 2.1, the strains in the ith interlayer can be expressed as

$$\bar{\varepsilon}_{z_i}^{(i)}(x,y,t)=\frac{-w^{(i+1)}(x,y,h_{i+1},t)+w^{(i)}(x,y,0,t)}{\Delta h},$$
$$\bar{\gamma}_{xz_i}^{(i)}(x,y,t)=\frac{-u^{(i+1)}(x,y,h_{i+1},t)+u^{(i)}(x,y,0,t)}{\Delta h}-\left.\frac{\partial w^{(i)}}{\partial x}\right|_{z_i=0},$$
$$\bar{\gamma}_{yz_i}^{(i)}(x,y,t)=\frac{-v^{(i+1)}(x,y,h_{i+1},t)+v^{(i)}(x,y,0,t)}{\Delta h}-\left.\frac{\partial w^{(i)}}{\partial y}\right|_{z_i=0},$$
$$i=1,2,\ldots,p-1. \tag{18}$$

Substituting Eqs. (14) and (17) into Eq. (18) yields the consistent conditions for displacements:

$$w^{(i+1)}(x,y,h_{i+1},t)=w^{(i)}(x,y,0,t)-\frac{\Delta h}{E(t)}\sigma_{z_i}^{(i)}(x,y,0,t),$$
$$u^{(i+1)}(x,y,h_{i+1},t)=u^{(i)}(x,y,0,t)-\frac{\Delta h}{G(t)}\tau_{xz_i}^{(i)}(x,y,0,t)+\Delta h\left.\frac{\partial w^{(i)}}{\partial x}\right|_{z_i=0},$$
$$v^{(i+1)}(x,y,h_{i+1},t)=v^{(i)}(x,y,0,t)-\frac{\Delta h}{G(t)}\tau_{yz_i}^{(i)}(x,y,0,t)+\Delta h\left.\frac{\partial w^{(i)}}{\partial y}\right|_{z_i=0},$$
$$i=1,2,\ldots,p-1. \tag{19}$$

2.5 Recursive matrix

The stress and displacement components in Eqs. (10) and (11) are rewritten in the matrix form as

$$\begin{bmatrix} u^{(i)}(x,y,z_i,t)\\ v^{(i)}(x,y,z_i,t)\\ w^{(i)}(x,y,z_i,t)\\ \sigma_{z_i}^{(i)}(x,y,z_i,t)\\ \tau_{xz_i}^{(i)}(x,y,z_i,t)\\ \tau_{yz_i}^{(i)}(x,y,z_i,t)\end{bmatrix}=\sum_{m=1}^{\infty}\sum_{n=1}^{\infty}\begin{bmatrix} U_{mn}^{(i)}(z_i,t)\cos(\alpha_m x)\sin(\beta_n y)\\ V_{mn}^{(i)}(z_i,t)\sin(\alpha_m x)\cos(\beta_n y)\\ W_{mn}^{(i)}(z_i,t)\sin(\alpha_m x)\sin(\beta_n y)\\ Z_{mn}^{(i)}(z_i,t)\sin(\alpha_m x)\sin(\beta_n y)\\ X_{mn}^{(i)}(z_i,t)\cos(\alpha_m x)\sin(\beta_n y)\\ Y_{mn}^{(i)}(z_i,t)\sin(\alpha_m x)\cos(\beta_n y)\end{bmatrix}, \tag{20}$$

in which the functions $U_{mn}^{(i)}(z_i,t)$, $V_{mn}^{(i)}(z_i,t)$, $W_{mn}^{(i)}(z_i,t)$, $Z_{mn}^{(i)}(z_i,t)$, $X_{mn}^{(i)}(z_i,t)$, and $Y_{mn}^{(i)}(z_i,t)$ can be determined by substituting Eqs. (10) and (11) into Eq. (20) as follows:

$$R_{mn}^{(i)}(z_i,t)=M_{mn}^{(i)}(z_i)\Omega_{mn}^{(i)}(t),\quad i=1,2,\ldots,p,\ m,n=1,2,3,\ldots, \tag{21}$$

where

$$R_{mn}^{(i)}(z_i,t)=\left[U_{mn}^{(i)}(z_i,t)\quad V_{mn}^{(i)}(z_i,t)\quad W_{mn}^{(i)}(z_i,t)\quad Z_{mn}^{(i)}(z_i,t)\quad X_{mn}^{(i)}(z_i,t)\quad Y_{mn}^{(i)}(z_i,t)\right]^{\mathrm{T}},$$
$$\Omega_{mn}^{(i)}(t)=\left[A_{mn}^{(i)}(t)\quad B_{mn}^{(i)}(t)\quad C_{mn}^{(i)}(t)\quad D_{mn}^{(i)}(t)\quad E_{mn}^{(i)}(t)\quad F_{mn}^{(i)}(t)\right]^{\mathrm{T}},$$

and

$$M_{mn}^{(i)}(z_i)=\begin{bmatrix} 0 & 0 & f_{mn}^{13}(z_i) & f_{mn}^{14}(z_i) & f_{mn}^{15}(z_i) & f_{mn}^{16}(z_i)\\ f_{mn}^{21}(z_i) & f_{mn}^{22}(z_i) & f_{mn}^{23}(z_i) & f_{mn}^{24}(z_i) & f_{mn}^{25}(z_i) & f_{mn}^{26}(z_i)\\ f_{mn}^{31}(z_i) & f_{mn}^{32}(z_i) & f_{mn}^{33}(z_i) & f_{mn}^{34}(z_i) & 0 & 0\\ f_{mn}^{41}(z_i) & f_{mn}^{42}(z_i) & f_{mn}^{43}(z_i) & f_{mn}^{44}(z_i) & 0 & 0\\ f_{mn}^{51}(z_i) & f_{mn}^{52}(z_i) & f_{mn}^{53}(z_i) & f_{mn}^{54}(z_i) & f_{mn}^{55}(z_i) & f_{mn}^{56}(z_i)\\ f_{mn}^{61}(z_i) & f_{mn}^{62}(z_i) & f_{mn}^{63}(z_i) & f_{mn}^{64}(z_i) & f_{mn}^{65}(z_i) & f_{mn}^{66}(z_i) \end{bmatrix},$$

in which the nonzero elements in the matrix are showed in Appendix. By letting $z_i=0$ and $z_i=h_i$ in Eq. (21), respectively, one has

$$R_{mn}^{(i)}(0,t)=M_{mn}^{(i)}(0)\Omega_{mn}^{(i)}(t),\qquad R_{mn}^{(i)}(h_i,t)=M_{mn}^{(i)}(h_i)\Omega_{mn}^{(i)}(t),$$
$$i=1,2,\ldots,p,\ m,n=1,2,3,\ldots \tag{22}$$

Eliminating $\Omega_{mn}^{(i)}(t)$ yields

$$R_{mn}^{(i)}(0,t)=M_{mn}^{(i)}(0)M_{mn}^{(i)}(h_i)^{-1}R_{mn}^{(i)}(h_i,t),\quad i=1,2,\ldots,p,\ m,n=1,2,3,\ldots \tag{23}$$

Similarly, the consistent conditions of Eqs. (17) and (19) can be given in the matrix form as follows:

$$R_{mn}^{(i+1)}(h_{i+1},t)=K_{mn}^{(i)}(t)R_{mn}^{(i)}(0,t),\quad i=1,2,\ldots,p-1,\ m,n=1,2,3,\ldots, \tag{24}$$

where

$$K_{mn}^{(i)}(t)=\begin{bmatrix} 1 & 0 & \alpha_m\Delta h & 0 & -\frac{\Delta h}{G(t)} & 0\\ 0 & 1 & \beta_n\Delta h & 0 & 0 & -\frac{\Delta h}{G(t)}\\ 0 & 0 & 1 & -\frac{\Delta h}{E(t)} & 0 & 0\\ 0 & 0 & 0 & 1 & 0 & 0\\ 0 & 0 & 0 & 0 & 1 & 0\\ 0 & 0 & 0 & 0 & 0 & 1 \end{bmatrix}.$$

Combining Eq. (23) with Eq. (24), one has

$$R_{mn}^{(p)}(0,t)=\left[\prod_{i=p}^{2}M_{mn}^{(i)}(0)M_{mn}^{(i)}(h_i)^{-1}K_{mn}^{(i-1)}(t)\right]M_{mn}^{(1)}(0)M_{mn}^{(1)}(h_1)^{-1}R_{mn}^{(1)}(h_1,t),$$
$$m,n=1,2,3,\ldots \tag{25}$$

The above equation indicates a direct relationship between the top surface and the bottom surface of the layered plate. We define

$$\begin{bmatrix} S_{mn}^{11}(t) & S_{mn}^{12}(t)\\ S_{mn}^{21}(t) & S_{mn}^{22}(t) \end{bmatrix}=\left[\prod_{i=p}^{2}M_{mn}^{(i)}(0)M_{mn}^{(i)}(h_i)^{-1}K_{mn}^{(i-1)}(t)\right]M_{mn}^{(1)}(0)M_{mn}^{(1)}(h_1)^{-1},$$
$$m,n=1,2,3,\ldots, \tag{26}$$

in which $S_{mn}^{11}(t)$, $S_{mn}^{12}(t)$, $S_{mn}^{21}(t)$, and $S_{mn}^{22}(t)$ are 3×3 sub-matrixes. Therefore, Eq. (25) becomes

$$\begin{bmatrix} U_{mn}^{(p)}(0,t) \\ V_{mn}^{(p)}(0,t) \\ W_{mn}^{(p)}(0,t) \\ Z_{mn}^{(p)}(0,t) \\ X_{mn}^{(p)}(0,t) \\ Y_{mn}^{(p)}(0,t) \end{bmatrix} = \begin{bmatrix} S_{mn}^{11}(t) & S_{mn}^{12}(t) \\ S_{mn}^{21}(t) & S_{mn}^{22}(t) \end{bmatrix} \begin{bmatrix} U_{mn}^{(1)}(h_1,t) \\ V_{mn}^{(1)}(h_1,t) \\ W_{mn}^{(1)}(h_1,t) \\ Z_{mn}^{(1)}(h_1,t) \\ X_{mn}^{(1)}(h_1,t) \\ Y_{mn}^{(1)}(h_1,t) \end{bmatrix}, \quad m,n = 1,2,3,\ldots \tag{27}$$

According to Eq. (20), the loading conditions of Eqs. (15) and (16) are rewritten as

$$\begin{aligned} &Z_{mn}^{(p)}(0,t) = 0, \qquad Z_{mn}^{(p)}(0,t) = 0, \\ &Z_{mn}^{(p)}(0,t) = -\frac{4}{ab}\int_0^a \int_0^b q(x,y) \sin\frac{m\pi x}{a} \sin\frac{n\pi y}{b} \mathrm{d}x\mathrm{d}y, \\ &Z_{mn}^{(1)}(h_1,t) = 0, \qquad X_{mn}^{(1)}(h_1,t) = 0, \qquad Y_{mn}^{(1)}(h_1,t) = 0, \quad m,n = 1,2,3,\ldots \end{aligned} \tag{28}$$

Decomposing Eq. (27) into two equations, one has

$$\begin{aligned} &S_{mn}^{11}(t) \begin{bmatrix} U_{mn}^{(1)}(h_1,t) \\ V_{mn}^{(1)}(h_1,t) \\ W_{mn}^{(1)}(h_1,t) \end{bmatrix} = \begin{bmatrix} U_{mn}^{(p)}(0,t) \\ V_{mn}^{(p)}(0,t) \\ W_{mn}^{(p)}(0,t) \end{bmatrix}, \\ &S_{mn}^{21}(t) \begin{bmatrix} U_{mn}^{(1)}(h_1,t) \\ V_{mn}^{(1)}(h_1,t) \\ W_{mn}^{(1)}(h_1,t) \end{bmatrix} = \begin{bmatrix} 0 \\ 0 \\ -\frac{4}{ab}\int_0^a \int_0^b q(x,y) \sin\frac{m\pi x}{a} \sin\frac{n\pi y}{b} \mathrm{d}x\mathrm{d}y \end{bmatrix}, \\ &m,n = 1,2,3,\ldots \end{aligned} \tag{29}$$

Solving the second equation in Eq. (29), one has

$$\begin{aligned} &\begin{bmatrix} U_{mn}^{(1)}(h_1,t) \\ V_{mn}^{(1)}(h_1,t) \\ W_{mn}^{(1)}(h_1,t) \end{bmatrix} = \left(S_{mn}^{21}(t)\right)^{-1} \begin{bmatrix} -\frac{4}{ab}\int_0^a \int_0^b q(x,y) \sin\frac{m\pi x}{a} \sin\frac{n\pi y}{b} \mathrm{d}x\mathrm{d}y \\ 0 \\ 0 \end{bmatrix}, \\ &m,n = 1,2,3,\ldots \end{aligned} \tag{30}$$

The solutions of stress and displacement components certainly exist, therefore, the six unknown coefficients in Eq. (21) should be uniquely determined, which means $|M_{mn}^{(i)}(z_i)| \neq 0$. Because $|K_{mn}^{(i)}(t)| = 1$, $|[\prod_{i=p}^{2} M_{mn}^{(i)}(0) M_{mn}^{(i)}(h_i)^{-1} K_{mn}^{(i-1)}(t)] M_{mn}^{(1)}(0) M_{mn}^{(1)}(h_1)^{-1}| \neq 0$ is certainly true. Thus, we conclude that the inverse matrix of $S_{mn}^{21}(t)$ always exists. Combining Eq. (23) with Eq. (24), one has

$$\begin{aligned} &R_{mn}^{(i)}(0,t) = \left[\prod_{j=i}^{1} M_{mn}^{(j)}(0)\left(M_{mn}^{(j)}(h_j)\right)^{-1} K(t)\right]\left(K(t)\right)^{-1} R_{mn}^{(1)}(h_1,t), \\ &i = 1,2,\ldots,p,\ m,n = 1,2,3,\ldots \end{aligned} \tag{31}$$

The undetermined coefficients for each layer are deduced as follows:

$$\Omega_{mn}^{(i)}(t) = \left(M_{mn}^{(i)}(0)\right)^{-1} R_{mn}^{(i)}(0,t), \quad i = 1,2,\ldots,p,\ m,n = 1,2,3,\ldots \tag{32}$$

Substituting these coefficients into Eqs. (10) and (11), the solution for stress and displacement components is finally obtained.

It should be pointed out that with the increase of the layer number p, only the computational cost in Eq. (26) correspondingly increases. As a result, the recursive matrix method has high efficiency in the present analysis.

3 Numerical results and discussion

Since the present solution is expressed by a double Fourier series with infinitely many terms, it should be truncated for practical calculation. The series terms for m and n are both truncated at N, i.e., $m, n = 1, 2, 3, \ldots, N$. The Poisson's ratio of the interlayer, denoted by μ_0, is assumed to be time-independent. Thus, $E(t) = 2(1+\mu_0)G(t)$. In the following numerical examples, the location of the plate is identified by the global Cartesian coordinates o-xyz. The locations in local Cartesian coordinates o_i-xyz_i can be transferred into global Cartesian coordinates o-xyz by the following relation:

$$z = z_i + (i-1)\Delta h + \sum_{j=1}^{i-1} h_j. \tag{33}$$

According to Assumption 2 given in Sect. 2.1, Eq. (33) can be simplified as

$$z = z_i + \sum_{j=1}^{i-1} h_j. \tag{34}$$

For brevity, four quantities are defined for the following analysis: $\sigma = \sigma_x^{(1)}$ at $x = 0.5a$, $y = 0.5b$, $z = h$, $\tau_1 = \tau_{xz}^{(1)}$ at $x = 0$, $y = 0.5b$, $z = h - h_1$, $\tau_2 = \tau_{xz}^{(2)}$ at $x = 0$, $y = 0.5b$, $z = h - h_1 - h_2$, and $w = w^{(1)}$ at $x = 0.5a$, $y = 0.5b$, $z = h$.

3.1 Convergence analysis

Since the present solution is expressed in a series, a convergence study should be carried out first. Consider a three-layer rectangle plate under the uniform load $q(x, y) = 1$ N/mm^2. The parameters are taken as $h_1 = h_3 = 20$ mm, $h_2 = 60$ mm, $\Delta h = 0.25$ mm, $E_1 = E_3 = 90$ GPa, $\mu_1 = \mu_3 = 0.3$, $\mu_2 = 0.2$, $\mu_0 = 0.3$, $t = 1$ year (3.1536×10^7 s), while a, b, and E_2 are variable. The viscoelastic interlayers are made of polyvinyl butyral with parameters taken from Galuppi and Royer-Carfagni (2012), as displayed in Table 1.

Table 2 gives the stress and displacement components for different series terms N from 1 to 15 with $a = 1000$ mm, $b = 750$ mm, $E_2 = 30$ GPa. From Table 2, a quick convergence property of present solution can be observed and the accuracy has at least two significant digits when $N = 15$. As a result, the series terms are taken up to $N = 15$ in all the following calculations.

Figures 3 and 4 respectively studied the influences of length–thickness ratio a/h and elasticity modulus ratio E_1/E_2 on convergence of the stress components $\sigma_x^{(3)}$, $\sigma_z^{(3)}$, $\tau_{xz}^{(2)}$, and $\tau_{xy}^{(2)}$. It can be observed that the convergence rates of the four components all increase with the decrease of a/h. With the increase of E_1/E_2, the convergence rate of $\sigma_x^{(3)}$ increases and that of $\tau_{xz}^{(2)}$ decreases. However, the convergence rates of $\sigma_z^{(3)}$ and $\tau_{xy}^{(2)}$ are less affected by E_1/E_2. Moreover, it is seen that $\tau_{xz}^{(2)}$ and $\tau_{xy}^{(2)}$ are monotonically convergent while $\sigma_x^{(3)}$ and $\sigma_z^{(3)}$ are oscillating convergent.

3.2 Comparison analysis

The present solution is compared with the solution from moderately thick plate theory based on Mindlin–Reissner (MR) hypothesis and the three-dimensional finite element (3DFE) solution. The MR solution is provided by the commercial software ANSYS using the two-dimensional SHELL-181 element, which considers the first-order transverse shear deformation of the plate. The 3DFE solution is obtained from ANSYS using the three-dimensional SOLID-185 element. Consider a two-layer square plate with $a = b$, under the uniform load $q(x, y) = 1$ N/mm^2. The geometric and material parameters are $h_1 = h_2 = 50$ mm, $\Delta h = 0.5$ mm, $E_1 = E_2$, $\mu_1 = \mu_2 = \mu_0 = 0.3$, and $G(t)$, as given in Table 1.

Table 1 Material parameters for polyvinyl butyral ($G(t) = G_\infty + \sum_{j=1}^{l} G_j e^{-t/\theta_{G,j}}$)

Term index j	G_j [MPa]	$\theta_{G,j}$ [s]
1	75.6426	3.256×10^{-11}
2	37.0677	4.949×10^{-9}
3	137.1552	7.243×10^{-8}
4	33.5140	9.864×10^{-6}
5	126.6048	2.806×10^{-3}
6	42.1950	1.644×10^{-1}
7	14.2162	2.265×10^{0}
8	3.5822	3.536×10^{1}
9	0.4538	9.368×10^{3}
10	0.1912	6.414×10^{5}
11	0.2893	4.135×10^{7}
$\infty(G_\infty)$	0.0880	–

Table 2 Convergence of the present results $\sigma_x^{(3)}, \sigma_y^{(3)}, \sigma_{z_i}^{(3)}, w^{(3)}$ at $x = 500$ mm, $y = 375$ mm, $z_3 = 20$ mm, and $\tau_{yz_i}^{(2)}, \tau_{xz_i}^{(2)}, \tau_{xy}^{(2)}, u^{(2)}, v^{(2)}$ at $x = 250$ mm, $y = 187.5$ mm, $z_2 = 10$ mm

N	$\sigma_x^{(3)}$	$\sigma_y^{(3)}$	$\sigma_{z_i}^{(3)}$	$\tau_{yz_i}^{(2)}$	$\tau_{xz_i}^{(2)}$	$\tau_{xy}^{(2)}$	$u^{(2)}$	$v^{(2)}$	$w^{(3)}$
1	49.36	67.12	−1.426	1.384	1.038	8.749	0.08354	0.1114	3.482
3	25.23	45.25	−0.8960	1.313	0.845	8.175	0.07933	0.1114	3.140
5	35.10	47.15	−0.9686	1.305	0.804	8.152	0.07900	0.1113	3.180
7	29.95	45.38	−0.9472	1.304	0.813	8.154	0.07903	0.1113	3.169
9	32.47	46.10	−0.9537	1.304	0.816	8.154	0.07904	0.1113	3.172
11	31.01	45.63	−0.9511	1.304	0.815	8.154	0.07904	0.1113	3.171
13	31.89	45.90	−0.9522	1.304	0.814	8.154	0.07904	0.1113	3.172
15	31.30	45.71	−0.9516	1.304	0.814	8.154	0.07904	0.1113	3.171

Note: the units of stresses and displacements are [MPa] and [mm], respectively.

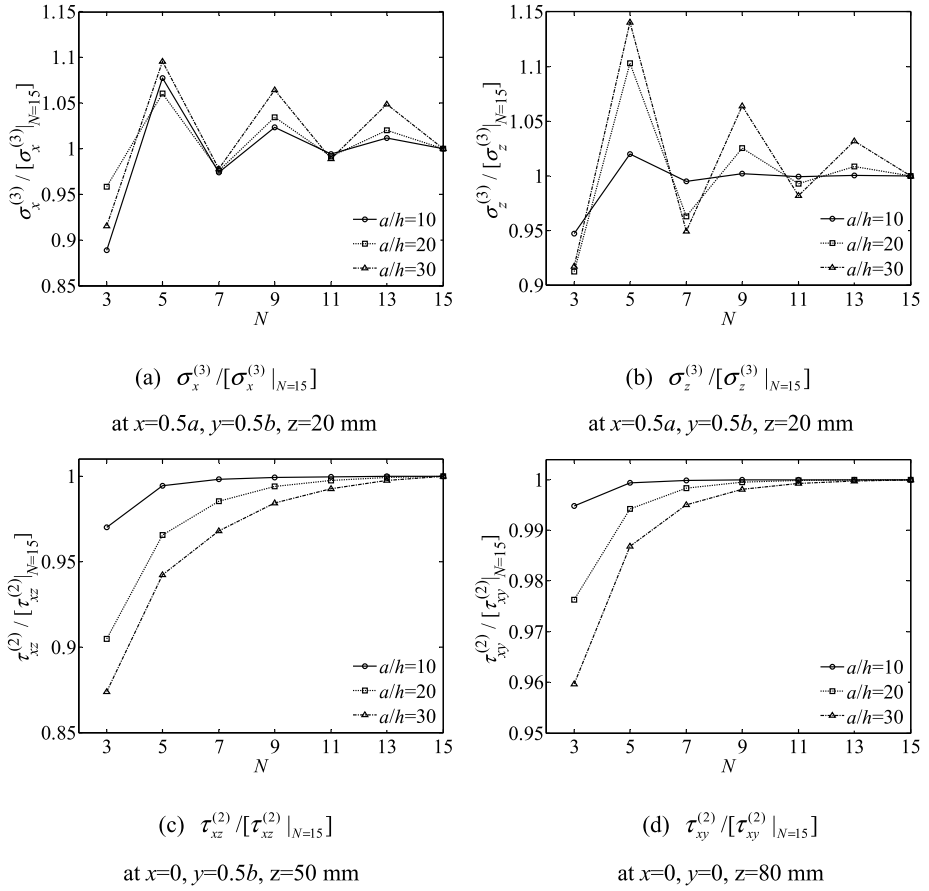

(a) $\sigma_x^{(3)}/[\sigma_x^{(3)}|_{N=15}]$ at x=0.5a, y=0.5b, z=20 mm

(b) $\sigma_z^{(3)}/[\sigma_z^{(3)}|_{N=15}]$ at x=0.5a, y=0.5b, z=20 mm

(c) $\tau_{xz}^{(2)}/[\tau_{xz}^{(2)}|_{N=15}]$ at x=0, y=0.5b, z=50 mm

(d) $\tau_{xy}^{(2)}/[\tau_{xy}^{(2)}|_{N=15}]$ at x=0, y=0, z=80 mm

Fig. 3 Convergence rates of the stress components with $a = b$ and $E_2 = 30$ GPa for different length–thickness ratios a/h

Comparisons of σ, τ_1, and w with $E_1 = 70$ GPa when $t = 1$ day (8.64×10^4 s) among the present, 3DFE and MR results for different length–thickness ratios a/h are displayed in Table 3. Close agreement between the present and 3DFE results can be observed. The errors are less than 1.5 % for all cases. It is seen from Table 3 that the MR results are close to the present ones for thin plate, however, the error increases as the length–thickness ratio increases. The errors of σ and w from MR theory respectively reach 9.61 % and 17.7 % when $a/h = 7.5$.

Figure 5 shows comparisons of σ, τ_1, and w with $E_1 = 8$ GPa and $a = 1000$ mm between the present solutions and the solutions from Foraboschi (2013a) where the interlayer was considered as fully elastic. It can be seen from Fig. 5 that the results from Foraboschi (2013a) are time-independent and are close to our results at the initial stage. However, σ and w in the present analysis increase with time while τ_1 decreases with time. They are all close to constants for the long time such as $t = 10^8$ s, which is greatly different from the solutions of Foraboschi (2013a). This demonstrates that the effects of viscosity cannot be ignored for layered plates with viscoelastic interlayers.

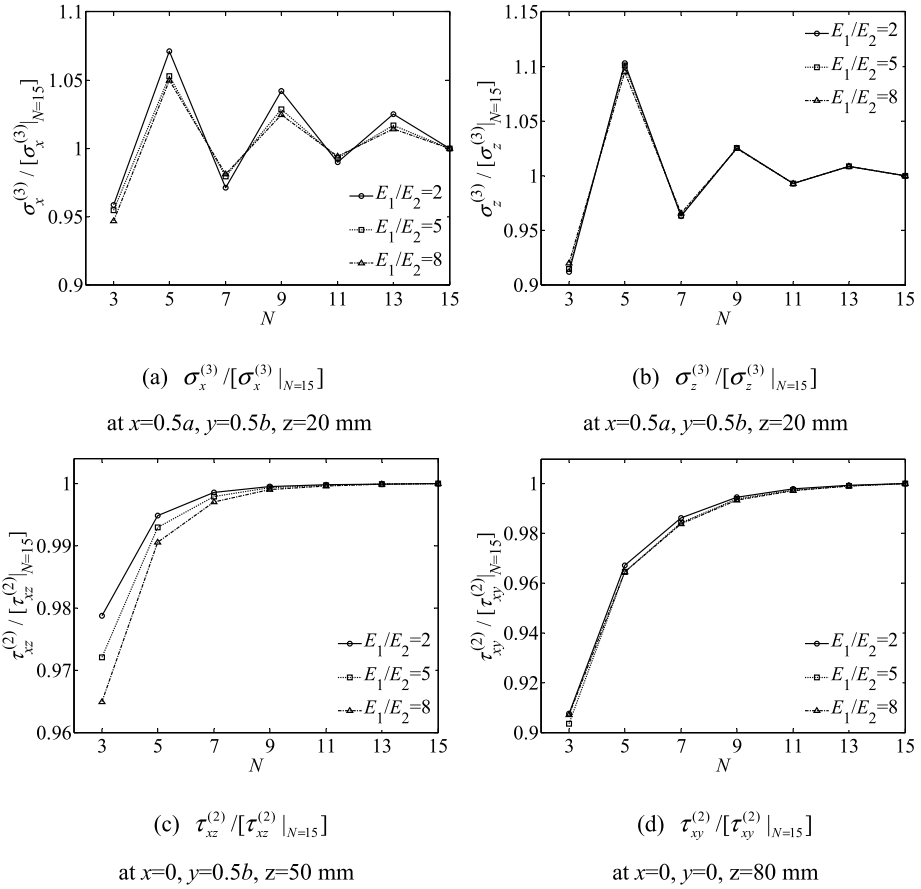

Fig. 4 Convergence rate of stress components with $a = b = 2000$ for different elasticity modulus ratios E_1/E_2

3.3 Parametric analysis

Consider a five-layer square plate under the sinusoidal load $q(x, y) = \sin(\pi x/a)\sin(\pi y/b)$ N/mm^2. The geometric and material parameters are assumed as $a = b = 1000$ mm, $h_i = 20$ mm, $E_i = 11$ GPa, $\mu_i = 0.3$, $\mu_0 = 0.3$, $(i = 1, 2 \ldots 5)$. $G(t)$ is given in Table 1.

Figure 6 plots the distributions of stress components $\sigma_x^{(i)}$, $\sigma_z^{(i)}$, $\tau_{xy}^{(i)}$, and $\tau_{xz}^{(i)}$ along the thickness and $\tau_{xz}^{(2)}$ in the x-o-y plane with $\Delta h = 0.25$ mm when $t = 1$ day (8.64×10^4 s), 1 year (3.1536×10^7 s), and 10 years (3.1536×10^8 s), respectively. It can be seen from Fig. 6 that the absolute values of $\sigma_x^{(i)}$ and $\tau_{xy}^{(i)}$ at the upper and lower surfaces of each plate layer increase with t. However, the variation of $\sigma_z^{(i)}$ with respect to t is small. $\tau_{xz}^{(i)}$ near the interlayer and $\tau_{xz}^{(2)}$ in the x-o-y plane, in absolute values, decrease with t.

Variations of σ, τ_2, and w with respect to t for three different interlayer thicknesses $\Delta h = 0.25$, 0.5 and 1 mm are respectively plotted in Fig. 7. It can be seen from Fig. 7 that σ and w increase with t, while τ_2 decreases with t. They all tend to be invariable after 10 years. Moreover, it is seen that σ and w increase as the interlayer thickness increases, while τ_2 decreases as the interlayer thickness increases.

Table 3 Comparisons of σ, τ_1, and w when $t = 1$ day (8.64×10^4 s) between the present, 3DFE and MR results for different length–thickness ratios a/h

a/h	Solutions	Present	3DFE	MR	Error for 3DFE (%)	Error for MR (%)
20	σ [Mpa]	192.4	192.3	192.8	0.0783	0.197
	τ_1 [MPa]	2.435	2.431	2.419	0.193	0.685
	w [mm]	31.21	31.16	31.42	0.155	0.700
12	σ [Mpa]	77.21	77.63	76.85	0.543	0.464
	τ_1 [MPa]	0.6479	0.6473	0.6429	0.103	0.774
	w [mm]	4.646	4.669	4.765	0.503	2.55
9	σ [MPa]	43.64	43.97	44.62	0.745	2.24
	τ_1 [MPa]	0.2901	0.2896	0.2878	0.164	0.788
	w [mm]	1.466	1.479	1.586	0.946	8.24
7.5	σ [Mpa]	28.66	29.03	31.42	1.27	9.61
	τ_1 [MPa]	0.1720	0.1713	0.1706	0.393	0.848
	w [mm]	0.6663	0.6755	0.7841	1.38	17.7

Note: Error for 3DFE denotes |(3DFE-Present)/Present|; error for MR denotes |(MR-Present)/Present|.

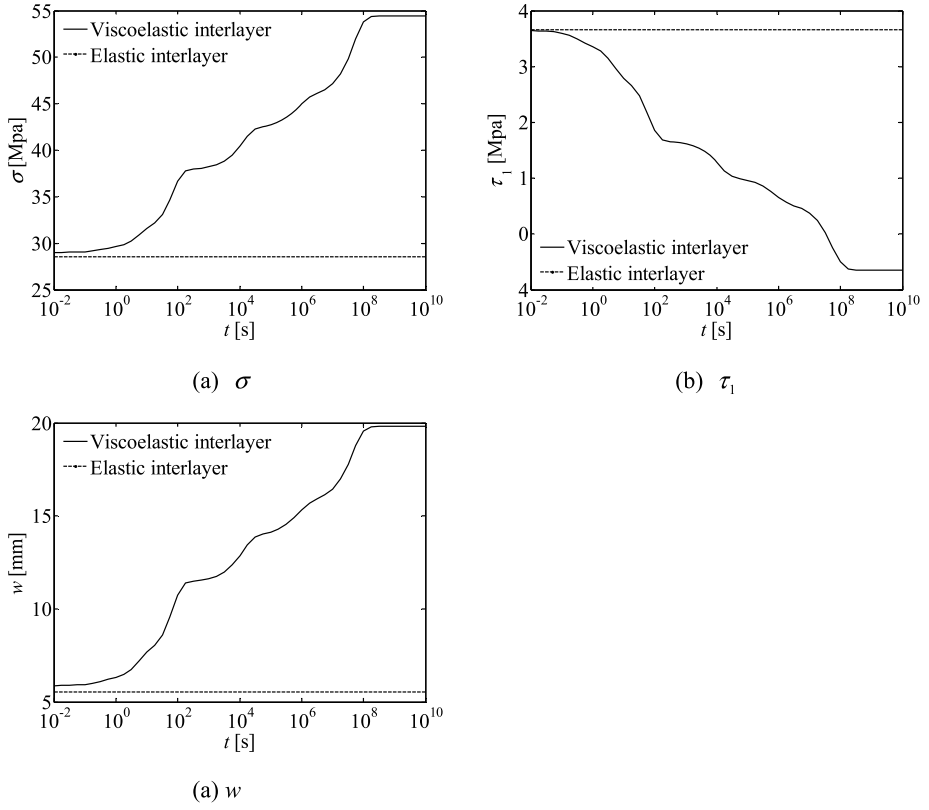

Fig. 5 Comparisons of σ, τ_1, and w between the present solutions and the solutions for the two-layer plate sandwiching an elastic interlayer

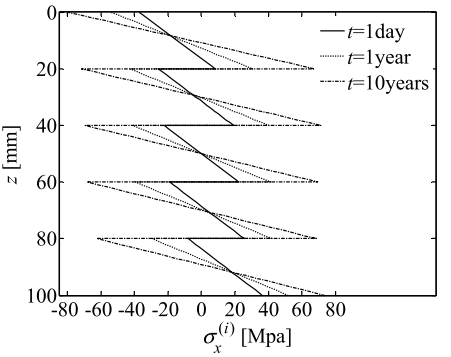

(a) $\sigma_x^{(i)}$ at x=500mm, y=500mm

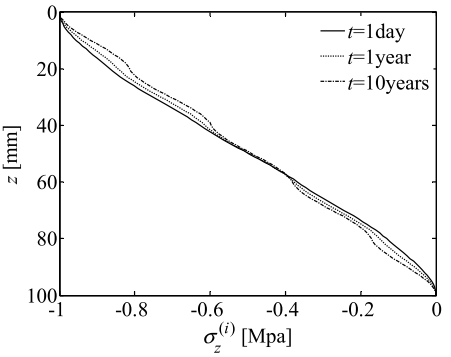

(b) $\sigma_z^{(i)}$ at x=500mm, y=500mm

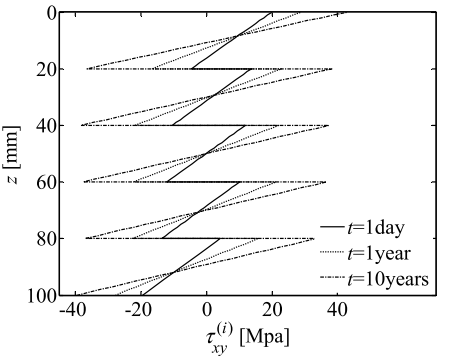

(c) $\tau_{xy}^{(i)}$ at x=0, y=0

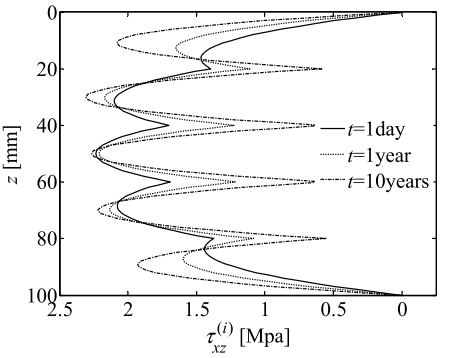

(d) $\tau_{xz}^{(i)}$ at x=0, y=500mm

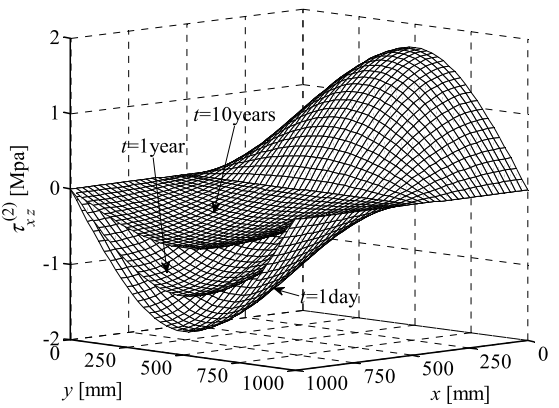

(e) $\tau_{xz}^{(2)}$ at z=60 mm

Fig. 6 Distributions of stress components with $\Delta h = 0.25$ mm when $t = 1$ day (8.64×10^4 s), 1 year (3.1536×10^7 s), and 10 years (3.1536×10^8 s), respectively

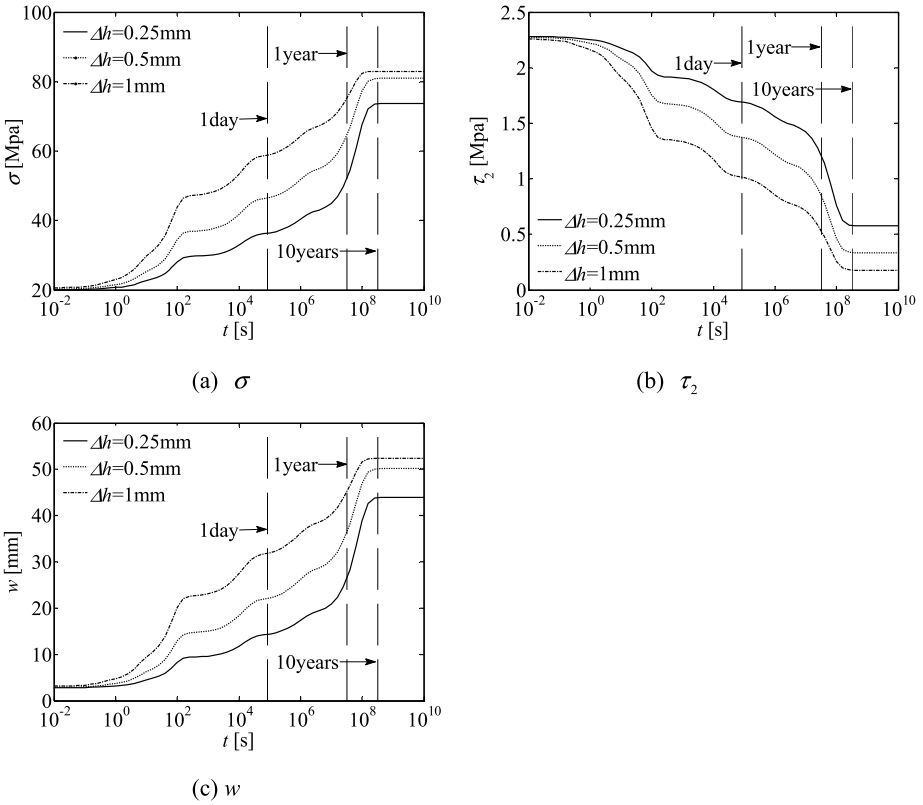

Fig. 7 Variations of σ, τ_2, and w with respect to t for $\Delta h = 0.25$, 0.5, and 1 mm, respectively

4 Concluding remarks

Based on the exact three-dimensional elasticity theory, an analytical solution for simply supported layered plates with viscoelastic interlayers under a transverse load is proposed. By using the recursive matrix technique, the solution is obtained efficiently. The following conclusions can be drawn:

1. The solution based on the Mindlin–Reissner plate theory is close to the present three-dimensional elasticity solution for thin plates; however, implies considerable errors for thick plates.
2. The present solution has good convergence. The convergence rate increases as the plate thickness increases.
3. The displacements and stresses of the plate vary with the time; however, they tend to be constants after a certain time.
4. The longitudinal normal stress and the deflection, in absolute values, increase as the interlayer thickness increases, while the absolute value of shear stress in the interlayer decreases as the interlayer thickness increases.

Acknowledgements This work is financially supported by the National Key Basic Research Program of China (Grant No. 2012CB026205) and the Key Project of National Natural Science Foundation of China

(Grant No. 51238003), the National Natural Science Foundation of China (Grant No. 51378255, 51208251) and the Transportation Science and Technology Project of Jiangsu Province (Grant No. 2014Y01).

Appendix

The nonzero elements of $M_{mn}^{(i)}(z_i)$ in Eq. (21) are obtained as follows:

$$f_{mn}^{13}(z_i) = \frac{\alpha_m \beta_n}{\phi_{mn}} z_i \sinh(\phi_{mn} z_i), \qquad f_{mn}^{14}(z_i) = \frac{\alpha_m \beta_n}{\phi_{mn}} z_i \cosh(\phi_{mn} z_i),$$

$$f_{mn}^{15}(z_i) = \beta_n \cosh(\phi_{mn} z_i), \qquad f_{mn}^{16}(z_i) = \beta_n \sinh(\phi_{mn} z_i),$$

$$f_{mn}^{21}(z_i) = \phi_{mn} \sinh(\phi_{mn} z_i), \qquad f_{mn}^{22}(z_i) = \phi_{mn} \cosh(\phi_{mn} z_i),$$

$$f_{mn}^{23}(z_i) = \frac{\lambda_i + 3G_i}{\lambda_i + G_i} \cosh(\phi_{mn} z_i) + \frac{(\beta_n)^2}{\phi_{mn}} z_i \sinh(\phi_{mn} z_i),$$

$$f_{mn}^{24}(z_i) = \frac{\lambda_i + 3G_i}{\lambda_i + G_i} \sinh(\phi_{mn} z_i) + \frac{(\beta_n)^2}{\phi_{mn}} z_i \cosh(\phi_{mn} z_i),$$

$$f_{mn}^{33}(z_i) = \beta_n z_i \cosh(\phi_{mn} z_i), \qquad f_{mn}^{34}(z_i) = \beta_n z_i \sinh(\phi_{mn} z_i),$$

$$f_{mn}^{41}(z_i) = 2\beta_n G_i \phi_{mn} \sinh(\phi_{mn} z_i), \qquad f_{mn}^{42}(z_i) = 2\beta_n G_i \phi_{mn} \cosh(\phi_{mn} z_i),$$

$$f_{mn}^{43}(z_i) = 2\beta_n G_i \left(\frac{G_i}{\lambda_i + G_i} \cosh(\phi_{mn} z_i) + \phi_{mn} z_i \sinh(\phi_{mn} z_i) \right),$$

$$f_{mn}^{44}(z_i) = 2\beta_n G_i \left(\frac{G_i}{\lambda_i + G_i} \sinh(\phi_{mn} z_i) + \phi_{mn} z_i \cosh(\phi_{mn} z_i) \right),$$

$$f_{mn}^{51}(z_i) = \alpha_m \beta_n G_i \cosh(\phi_{mn} z_i), \qquad f_{mn}^{52}(z_i) = \alpha_m \beta_n G_i \sinh(\phi_{mn} z_i),$$

$$f_{mn}^{53}(z_i) = \beta_n G_i \left(\frac{\alpha_m}{\phi_{mn}} \sinh(\phi_{mn} z_i) + 2\alpha_m z_i \cosh(\phi_{mn} z_i) \right),$$

$$f_{mn}^{54}(z_i) = \beta_n G_i \left(\frac{\alpha_m}{\phi_{mn}} \cosh(\phi_{mn} z_i) + 2\alpha_m z_i \sinh(\phi_{mn} z_i) \right),$$

$$f_{mn}^{55}(z_i) = \beta_n \phi_{mn} G_i \sinh(\phi_{mn} z_i), \qquad f_{mn}^{56}(z_i) = \beta_n \phi_{mn} G_i \cosh(\phi_{mn} z_i),$$

$$f_{mn}^{61}(z_i) = \left[(\beta_n)^2 + (\phi_{mn})^2 \right] G_i \cosh(\phi_{mn} z_i),$$

$$f_{mn}^{62}(z_i) = \left[(\beta_n)^2 + (\phi_{mn})^2 \right] G_i \sinh(\phi_{mn} z_i),$$

$$f_{mn}^{63}(z_i) = \left[\left(\frac{\lambda_i + 3G_i}{\lambda_i + G_i} \phi_{mn} + \frac{(\beta_n)^2}{\phi_{mn}} \right) \sinh(\phi_{mn} z_i) + 2(\beta_n)^2 z_i \cosh(\phi_{mn} z_i) \right] G_i,$$

$$f_{mn}^{64}(z_i) = \left[\left(\frac{\lambda_i + 3G_i}{\lambda_i + G_i} \phi_{mn} + \frac{(\beta_n)^2}{\phi_{mn}} \right) \cosh(\phi_{mn} z_i) + 2(\beta_n)^2 z_i \sinh(\phi_{mn} z_i) \right] G_i,$$

$$f_{mn}^{65}(z_i) = -\alpha_m \phi_{mn} G_i \sinh(\phi_{mn} z_i), \qquad f_{mn}^{66}(z_i) = -\alpha_m \phi_{mn} G_i \sinh(\phi_{mn} z_i).$$

References

Alipour, M.M.: An analytical approach for bending and stress analysis of cross/angle-ply laminated composite plates under arbitrary non-uniform loads and elastic foundations. Arch. Civ. Mech. Eng. **16**(2), 193–210 (2016)

Arzoumanidis, G.A., Liechti, K.M.: Linear viscoelastic property measurement and its significance for some nonlinear viscoelasticity models. Mech. Time-Depend. Mater. **7**(3–4), 209–250 (2003)

Boltzmann, L.: Sitzungsber. Kaiserl. Akad. Wiss. Wien, Math.-Naturwiss. **70**, 275–285 (1874)

Dallot, J., Sab, K.: Limit analysis of multi-layered plates. Part I: the homogenized Love–Kirchhoff model. J. Mech. Phys. Solids **56**(2), 561–580 (2008)

Del Linz, P., Liang, X., Hooper, P.A., Wang, L.Z., Dear, J.P.: An analytical solution for pre-crack behaviour of laminated glass under blast loading. Compos. Struct. **144**, 156–164 (2016)

Ferreira, A.J.M., Roque, C.M.C., Martins, P.A.L.S.: Analysis of composite plates using higher-order shear deformation theory and a finite point formulation based on the multiquadric radial basis function method. Composites, Part B, Eng. **34**(7), 627–636 (2003)

Foraboschi, P.: Analytical model for laminated-glass plate. Composites, Part B, Eng. **43**(5), 2094–2106 (2012)

Foraboschi, P.: Three-layered sandwich plate: exact mathematical model. Composites, Part B, Eng. **45**(1), 1601–1612 (2013a)

Foraboschi, P.: Layered plate with discontinuous connection: exact mathematical model. Composites, Part B, Eng. **47**, 365–378 (2013b)

Foraboschi, P.: Three-layered plate: elasticity solution. Composites, Part B, Eng. **60**, 764–776 (2014)

Galuppi, L., Royer-Carfagni, G.: Laminated beams with viscoelastic interlayer. Int. J. Solids Struct. **49**(18), 2637–2645 (2012)

Galuppi, L., Royer-Carfagni, G.: The design of laminated glass under time-dependent loading. Int. J. Mech. Sci. **68**, 67–75 (2013)

Galuppi, L., Royer-Carfagni, G.: Buckling of three-layered composite beams with viscoelastic interaction. Compos. Struct. **107**, 512–521 (2014)

Golmakani, M.E., Mehrabian, M.: Nonlinear bending analysis of ring-stiffened circular and annular general angle-ply laminated plates with various boundary conditions. Mech. Res. Commun. **59**, 42–50 (2014)

Gregory, R.D., Wan, F.Y.: Correct asymptotic theories for the axisymmetric deformation of thin and moderately thick cylindrical shells. Int. J. Solids Struct. **30**(14), 1957–1981 (1993)

Guedes, R.M., Marques, A.T., Cardon, A.: Analytical and experimental evaluation of nonlinear viscoelastic-viscoplastic composite laminates under creep, creep-recovery, relaxation and ramp loading. Mech. Time-Depend. Mater. **2**(2), 113–128 (1998)

Hadigheh, S.A., Gravina, R.J.: Generalization of the interface law for different FRP processing techniques in FRP-to-concrete bonded interfaces. Composites, Part B, Eng. **91**, 399–407 (2016)

Hu, H.S., Nie, J.G., Wang, Y.H.: Shear capacity of concrete-filled steel plate composite coupling beams. J. Constr. Steel Res. **118**, 76–90 (2016)

Kant, T., Swaminathan, K.: Analytical solutions for the static analysis of laminated composite and sandwich plates based on a higher order refined theory. Compos. Struct. **56**(4), 329–344 (2002)

Kaplunov, J.D., Kossovich, L.Y., Nolde, E.V.: Dynamics of Thin Walled Elastic Bodies. Academic Press, San Diego (1998)

Khdeir, A.A.: Free vibration and buckling of symmetric cross-ply laminated plates by an exact method. J. Sound Vib. **126**(3), 447–461 (1988)

Kim, J., Sholar, G.A., Kim, S.: Determination of accurate creep compliance and relaxation modulus at a single temperature for viscoelastic solids. J. Mater. Civ. Eng. **20**(2), 147–156 (2008)

Kim, S.E., Thai, H.T., Lee, J.: A two variable refined plate theory for laminated composite plates. Compos. Struct. **89**(2), 197–205 (2009)

Kirchhoff, G.R.: Über das Gleichgewicht und die Bewegung einer elastischen Scheibe. J. Reine Angew. Math. **40**, 51–88 (1850)

Le-Anh, L., Nguyen-Thoi, T., Ho-Huu, V., Dang-Trung, H., Bui-Xuan, T.: Static and frequency optimization of folded laminated composite plates using an adjusted Differential Evolution algorithm and a smoothed triangular plate element. Compos. Struct. **127**, 382–394 (2015)

Li, J., Zheng, B.L., Yang, Q., Hu, X.J.: Analysis on time-dependent behavior of laminated functionally graded beams with viscoelastic interlayer. Compos. Struct. **107**, 30–35 (2014)

Mantari, J.L., Ore, M.: Free vibration of single and sandwich laminated composite plates by using a simplified FSDT. Compos. Struct. **132**, 952–959 (2015)

Matsunaga, H.: Vibration and stability of cross-ply laminated composite plates according to a global higher-order plate theory. Compos. Struct. **48**(4), 231–244 (2000)

Mindlin, R.D.: Influence of rotary inertia and shear on flexural motions of isotropic elastic plates. J. Appl. Mech. **18**, 31–38 (1951)
Neto, P., Alfaiate, J., Dias-da-Costa, D., Vinagre, J.: Mixed-mode fracture and load misalignment on the assessment of FRP-concrete bond connections. Compos. Struct. **135**, 49–60 (2016)
Neville, A.M., Dilger, W.H., Brooks, J.J.: Creep of Plain and Structural Concrete. Longman, New York (1983)
Othman, H., Marzouk, H.: An experimental investigation on the effect of steel reinforcement on impact response of reinforced concrete plates. Int. J. Impact Eng. **88**, 12–21 (2016)
Pagano, N.J.: Exact solutions for composite laminates in cylindrical bending. J. Compos. Mater. **3**(3), 398–411 (1969)
Pagano, N.J.: Exact solutions for rectangular bidirectional composites and sandwich plates. J. Compos. Mater. **4**(1), 20–34 (1970)
Park, I., Lee, U.: Spectral element modeling and analysis of the transverse vibration of a laminated composite plate. Compos. Struct. **134**, 905–917 (2015)
Reddy, J.N.: A simple higher-order theory for laminated composite plates. J. Appl. Mech. **51**(4), 745–752 (1984)
Reissner, E.: The effect of transverse shear deformation on the bending of elastic plates. J. Appl. Mech. **12**, 69–77 (1945)
Reissner, E.: On the analysis of first and second-order shear deformation effects for isotropic elastic plates. J. Appl. Mech. **47**(4), 959–961 (1980)
Romanoff, J., Varsta, P.: Bending response of web-core sandwich plates. Compos. Struct. **81**(2), 292–302 (2007)
Shafaei, S., Ayazi, A., Farahbod, F.: The effect of concrete panel thickness upon composite steel plate shear walls. J. Constr. Steel Res. **117**, 81–90 (2016)
Srinivas, S., Rao, A.K.: Bending, vibration and buckling of simply supported thick orthotropic rectangular plates and laminates. Int. J. Solids Struct. **6**(11), 1463–1481 (1970)
Swaminathan, K., Patil, S.S.: Higher order refined computational model with 12 degrees of freedom for the stress analysis of antisymmetric angle-ply plates—analytical solutions. Compos. Struct. **80**(4), 595–608 (2007)
Teng, X., Zhang, Y.X., Lin, X.: Two new composite plate elements with bond–slip effect for nonlinear finite element analyses of FRP-strengthened concrete slabs. Comput. Struct. **148**, 35–44 (2015)
Thai, H.T., Choi, D.H.: Size-dependent functionally graded Kirchhoff and Mindlin plate models based on a modified couple stress theory. Compos. Struct. **95**, 142–153 (2013)
Wang, C.M., Ang, K.K., Yang, L., Watanabe, E.: Free vibration of skew sandwich plates with laminated facings. J. Sound Vib. **235**(2), 317–340 (2000)
Williams, T.O., Addessio, F.L.: A general theory for laminated plates with delaminations. Int. J. Solids Struct. **34**(16), 2003–2024 (1997)
Wu, P., Zhou, D., Liu, W.: 2-D elasticity solution of layered composite beams with viscoelastic interlayers. Mech. Time-Depend. Mater. **20**(1), 65–84 (2016a)
Wu, P., Zhou, D., Liu, W., Wan, L., Liu, D.: Elasticity solution of two-layer beam with a viscoelastic interlayer considering memory effect. Int. J. Solids Struct. **94–95**, 76–86 (2016b)
Xu, T., He, Z.J., Tang, C.A., Zhu, W.C., Ranjith, P.G.: Finite element analysis of width effect in interface debonding of FRP plate bonded to concrete. Finite Elem. Anal. Des. **93**, 30–41 (2015)
Yan, J.B., Wang, J.Y., Liew, J.R., Qian, X., Li, Z.X.: Punching shear behavior of steel–concrete–steel sandwich composite plate under patch loads. J. Constr. Steel Res. **121**, 50–64 (2016)
Yang, X.D., Yu, T.J., Zhang, W., Qian, Y.J., Yao, M.H.: Damping effect on supersonic panel flutter of composite plate with viscoelastic mid-layer. Compos. Struct. **137**, 105–113 (2016)
Zhang, C., Wang, J.L.: Viscoelastic analysis of FRP strengthened reinforced concrete beams. Compos. Struct. **93**(12), 3200–3208 (2011)
Zhu, H., Khanna, S.K.: Dynamic response of a novel laminated glass panel using a transparent glass fiber-reinforced composite interlayer under blast loading. Int. J. Impact Eng. **89**, 14–24 (2016)